(Received 13 August 2025, Accepted 26 November 2025, Scheduled 12 December 2025)

# Integral Sliding Mode Speed Control of PMSM Based on Novel Fuzzy Exponential Reaching Law

Zhonggen Wang[1], Jinpeng Ma[1,*], and Wenyan Nie[2]

[1] School of Electrical and Information Engineering, Anhui University of Science and Technology, Huainan 232001, China
[2] School of Mechanical and Electrical Engineering, Huainan Normal University, Huainan 232001, China

**ABSTRACT:** To enhance the speed control performance of permanent magnet synchronous motor (PMSM) drive systems, a novel sliding mode control (SMC) strategy based on a new fuzzy exponential reaching law (NFERL) is proposed. The law enhances the traditional exponential reaching law by introducing a system-state-dependent power term and a fuzzy term that adapts the reaching speed based on the sliding mode function. A hyperbolic tangent function replaces the high-frequency switching term to suppress chattering. This control strategy helps reduce current ripples and torque pulsations, and improves the stability and response speed of system operation. Additionally, to address the issue that the system is susceptible to unknown disturbances, a sliding mode disturbance observer (SMDO) is designed to estimate the total disturbance of the system, and the estimated disturbance is fed forward into a composite speed controller. Finally, the introduced control strategy is validated using MATLAB/Simulink simulations and a motor experimental platform. Both simulated and experimental results demonstrate that the new reaching law effectively reduces the startup speed overshoot of the PMSM compared to the traditional law, while also achieving faster convergence, reduced chattering, and superior anti-disturbance performance.

## 1. INTRODUCTION

Permanent Magnet Synchronous Motors (PMSMs) have become core power components in industrial drives [1–3], new energy vehicles [4, 5], and aerospace applications [6] due to their high-power density, high operational efficiency, and precise controllability. However, PMSM drive systems are characterized by strong nonlinearity, multi-variable coupling, and susceptibility to parameter variations, external load disturbances, and modeling dynamics, rendering conventional vector control methods [7] inadequate in complex operating conditions with issues such as sluggish dynamic response and insufficient anti-interference capability.

To address the limitations of traditional PI controllers and enhance control strategy performance, researchers have introduced modern control theories such as adaptive fuzzy systems [8], model predictive control [9, 10], disturbance estimation techniques [11–13], and sliding mode control (SMC) [14–16]. Among them, SMC has garnered significant attention in the control field due to its simple structure, low dependency on model accuracy, and strong robustness. However, in conventional SMC, chattering caused by system discontinuity and high-gain switching terms in the sliding mode reaching law adversely affects control performance. Even in integral SMC, the trade-off between steady-state error and dynamic performance remains unresolved. Consequently, various optimization methods have been proposed. Ref. [17] designs an anti-windup sliding surface that shortens dynamic response time by adjusting the reaching speed. Yet, this approach remains susceptible to external disturbances due to the presence of speed differential terms in the SMC structure. Ref. [18] proposes a fast recursive terminal SMC strategy, enabling system initialization on the sliding surface, which reduces convergence time while mitigating noise and vibration effects. Since chattering primarily stems from non-ideal convergence trajectories toward the sliding surface, a process determined by the reaching law optimizing the reaching law is crucial for chattering suppression. Ref. [19] incorporates sliding variables into a high-order SMC reaching law and replaces switching functions with hyperbolic tangent functions, effectively mitigating chattering in speed regulation systems. Ref. [20] introduces a double-layer fast terminal sliding mode structure to enhance response speed, though its numerous parameters pose tuning challenges. Ref. [21] develops a sliding mode disturbance observer that improves anti-interference capability and tracking accuracy by compensating for speed loop disturbances, albeit with relatively slow convergence speed.

Recent research on fuzzy sliding mode control has made notable progress, with [22] proposing a fixed-time adaptive fuzzy control method based on filters and observers that effectively handle uncertain functions in systems. Ref. [23] designs a controller using a novel adaptive sliding mode reaching law to enhance system response speed and suppress torque-speed pulsation. Existing exponential reaching laws cannot simultaneously achieve high-speed convergence and low chattering under varying load conditions; this study introduces a fuzzy-based adaptation mechanism to resolve this trade-off. Based on the above analysis, this paper proposes a sliding mode control strategy for permanent magnet synchronous motors, further optimizing the dynamic performance of PMSM control systems, using a novel

* Corresponding author: Jinpeng Ma (jpma888@163.com).

fuzzy exponential reaching law. The main contributions are as follows:

(1) A fuzzy exponential reaching law for integral sliding mode control is suggested. The parameter in the function of this law is fuzzified. Furthermore, a sliding mode observer is designed by integrating the NFERL with an integral sliding mode surface. Theoretical analysis demonstrates that the proposed reaching law effectively resolves the inherent conflict between rapid convergence and chattering suppression, reduces overshoot, and significantly shortens the system convergence time.

(2) A new disturbance observer is designed to provide feedforward compensation for disturbances in the sliding mode controller, significantly enhancing the disturbance rejection capability and robustness of the speed control system.

(3) The feasibility of the innovated integral sliding mode speed control method, which is based on the fuzzy exponential reaching law, is validated through MATLAB/Simulink simulations and a physical PMSM drive experimental platform. Experimental results confirm that the proposed control strategy achieves superior dynamic and steady-state performance.

## 2. PMSM CONTROL THEORY

### 2.1. PMSM Mathematical Model

Under standard electromechanical modeling assumptions, the mathematical model of PMSMs can be systematically derived from electromagnetic field principles. This derivation requires three fundamental premises to be satisfied: symmetrical three-phase armature windings, negligible magnetic saturation effects, and the exclusion of core loss mechanisms. Based on coordinate transformation theory, the dynamic equations for stator currents in the rotor-oriented $d$-$q$ reference frame are expressed as follows:

$$\begin{cases} U_d = R_s i_d + \frac{\mathrm{d}\psi_d}{\mathrm{d}t} - \omega_e \psi_q \\ U_q = R_s i_q + \frac{\mathrm{d}\psi_q}{\mathrm{d}t} + \omega_e \psi_d \end{cases} \tag{1}$$

The stator flux linkage equations in the $d$-$q$ reference frame are:

$$\begin{cases} \psi_d = L_d i_d + \psi_f \\ \psi_q = L_q i_q \end{cases} \tag{2}$$

The torque equation for PMSMs in the $d$-$q$ reference frame is:

$$T_e = \frac{3}{2} p_n i_q \left[ i_d \left( L_d - L_q \right) + \psi_f \right] \tag{3}$$

where $U_d$, $U_q$, $i_q$, and $i_d$ are the orthogonal components of stator voltage and stator current in the coordinate system; $L_d$ and $L_q$ are $d$-$q$ orthogonal components of inductance; $R_s$ is the stator resistance; $\omega_e$ is the electrical angular velocity, and $\omega_e = p_n \omega_m$; $\omega_m$ is the mechanical angular velocity of the motor; $p_n$ is the number of pole pairs; $\psi_f$ is the magnetic flux of the permanent magnet; and $T_e$ is the electromagnetic torque. The surface-mounted permanent magnet synchronous motor is taken as the control object, where $L_d = L_q$ holds. Adopt the $i_d = 0$ based magnetic field orientation control strategy to maximize the output electromagnetic torque.

The torque equation can be rewritten as:

$$T_e = \frac{3}{2} p_n \psi_f i_q \tag{4}$$

The motor motion equation is:

$$J \frac{\mathrm{d}\omega_m}{\mathrm{d}t} = T_e - T_L - B\omega_m \tag{5}$$

where $J$ is the moment of inertia, $T_L$ the load torque, and $B$ the damping factor.

### 2.2. New Fuzzy Exponential Sliding Mode Reaching Law

To address the inherent trade-off between convergence speed and chattering in traditional exponential reaching laws and to enhance the performance of control systems, this paper proposes a new fuzzy exponential sliding mode reaching law (NFESMRL).

$$\begin{gathered} \dot{s} = -f(x) \tanh(\lambda s) - k\,|s|\, e^{(-\eta x)} \\ f(x) = \begin{cases} \frac{\varepsilon}{k}, & |x| \geq \delta \\ \frac{k|x|}{|x|^m + 1}, & |x| < \delta \end{cases} \end{gathered} \tag{6}$$

where $x$ is the system state variable; $\lim\limits_{t \to \infty} |x| = 0$; $\varepsilon$, $k$, $m$, $\lambda$, $\eta$ are the coefficients to be determined, and $\varepsilon > 0$, $k > 0$, $0 < m < 1$, $\eta > 0$, $0 < \lambda < 1$.

The new fuzzy exponential sliding mode reaching law introduces a function term $f(x)$ about the state of the system and a reaching term $k|s|e^{(-\eta x)}$ about the function of the sliding mode surface. As the state of the system moves away from the sliding mode surface, the arrival velocity consists of two parts, the new fuzzy exponential sliding mode reaching law $f(x)$ and the enhanced exponential reaching term $k|s|e^{(-\eta x)}$, which shorten the time during the arrival process by moving from a slower to a faster velocity. When $|x|$ approaches the sliding mode surface, i.e., $|x| > 0$, the arrival speed is determined by $f(x)\tanh(\lambda s)$. Under the action of the sliding mode control rate, $|x|$ enters the sliding mode surface and moves toward the origin, and this process makes $-f(x)\tanh(\lambda s) - k|s|e^{(-\eta x)}$ gradually converge to 0 and finally stabilize at the origin, thus reducing the sliding mode vibration. In addition, the sign function $\mathrm{sign}(s)$ is replaced by the hyperbolic tangent function $\tanh(\lambda s)$, which weakens the effect of the high-frequency switching gain near the sliding mode surface on the system chattering.

### 2.3. Sliding Mode Fuzzy Gain Design

To optimize speed control performance, the parameter $m$ in the controller's new function $f(x)$ can be adaptively adjusted via designed fuzzy rules. Here, $m(m > 0)$ is the basic smoothing parameter dynamically adjusted by fuzzy rules; $k \in [0, 1]$ is the weight coefficient adapted based on system error; and $\lambda > 0$ is a fixed high-frequency attenuation factor $\lambda = 0.1$. When the

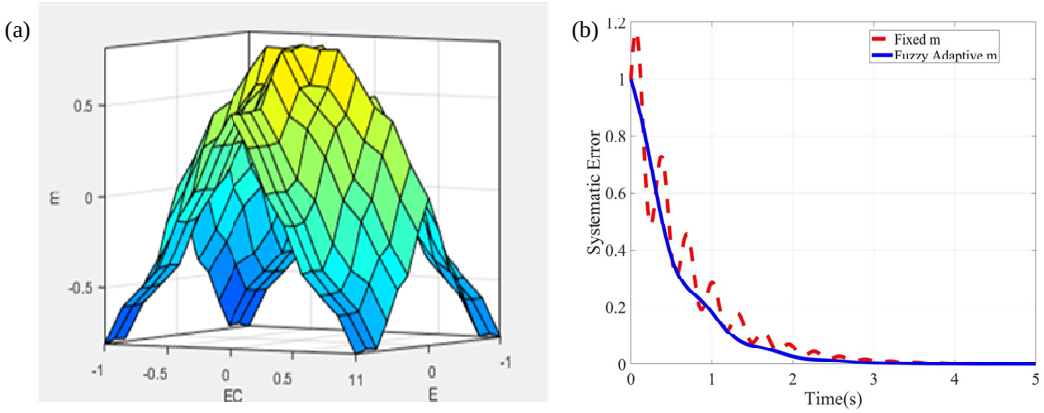


**FIGURE 1**. Quantitative presentation of fuzzy rules. (a) Input output relationship. (b) Systematic error correction process.

**TABLE 1**. Input variable.

| Fuzzy set | $E$ | $EC$ |
|---|---|---|
| NB | $(-1.0, -1.0, -0.6)$ | $(-1.0, -1.0, -0.6)$ |
| NM | $(-0.8, -0.6, -0.3)$ | $(-0.8, -0.6, -0.3)$ |
| NS | $(-0.4, -0.2, 0.0)$ | $(-0.4, -0.2, 0.0)$ |
| ZO | $(-0.1, 0.0, 0.1)$ | $(-0.1, 0.0, 0.1)$ |
| PS | (0.0, 0.2, 0.4) | (0.0, 0.2, 0.4) |
| PM | (0.3, 0.6, 0.8) | (0.3, 0.6, 0.8) |
| PB | (0.6, 1.0, 1.0) | (0.6, 1.0, 1.0) |

**TABLE 2**. Output variable.

| Fuzzy set | $m$ |
|---|---|
| VS | (0.0, 0.0, 0.25) |
| S | (0.1, 0.3, 0.5) |
| M | (0.4, 0.5, 0.6) |
| L | (0.5, 0.7, 0.9) |
| VL | (0.75, 1.0, 1.0) |

system state is far from the sliding mode surface, $m$ increases, when it is near the surface, $m$ decreases.

Fuzzy sets {NB, NM, NS, ZO, PS, PM, PB} are used for input variables $E$ (error) and $EC$ (error change rate). The error $e$ ranges over $[-1, 1]$ with fuzzy sets defined as: NB (Negative Big), NM (Negative Medium), NS (Negative Small), ZO (Zero), PS (Positive Small), PM (Positive Medium), PB (Positive Big). The error change rate $EC$ also ranges over $[-1, 1]$. The output variable $m$ uses fuzzy sets {VS, S, M, L, VL} corresponding to Very Small, Small, Medium, Large, and Very Large.

Input and output variable definitions, position error $e = \frac{\omega_{ref}-\omega_m}{100}$, error change rate $ec = \frac{de}{dt} \cdot \frac{1}{50}$, output parameters $m$ smoothing coefficient (range: [0, 1]).

The parameterized definitions of the membership functions are as follows: the trigonometric function parameters $(a, b, c)$ for the input variable are shown in Table 1, and the membership functions for the output variable are shown in Table 2.

The fuzzy rules are presented in Table 3, and the membership functions of all variables are trigonometric functions. The fuzzy reasoning algorithm is based on the Mamdani method.

**TABLE 3**. Fuzzy rules.

| $E/EC$ | NB | NM | NS | ZO | PS | PM | PB |
|---|---|---|---|---|---|---|---|
| NB | VS | VS | S | M | S | VS | VS |
| NM | S | S | M | L | M | S | S |
| NS | M | M | L | VL | L | M | M |
| ZO | L | L | VL | VL | VL | L | L |
| PS | M | M | L | VL | L | M | M |
| PM | S | S | M | L | M | S | S |
| PB | VS | VS | S | M | S | VS | VS |

The barycenter method is used for defuzzification to obtain the crisp output. The variation of the output variable $m$ is illustrated, and the fuzzy term dynamically adjusts the reaching speed by quickly correcting the systematic error in Figure 1.

## 3. DESIGN OF COMPOSITE SPEED CONTROLLER

### 3.1. Based NFESMRL Speed Controller

Based on the mathematical model of the permanent magnet synchronous motor, Eqs. (1) to (5), and considering the total perturbation due to external load variations and internal parameter changes denoted as $d(t)$, the speed control model of the motor can be derived as follows:

$$\dot{\omega}_m = \frac{3p_n\psi_f}{2J} i_q - \frac{B}{J}\omega_m - \frac{1}{J}d(t) \tag{7}$$

In order to facilitate the design of the new fuzzy exponential sliding mode reaching law controller, the velocity error is defined as:

$$e = \omega_{ref} - \omega_m \tag{8}$$

where $\omega_{ref}$ is the given rotational speed, and $\omega_m$ is the actual rotational speed.

The integral sliding mode surface function is chosen to be:

$$s = e + c\int_0^t edt + \mu\dot{e} \tag{9}$$

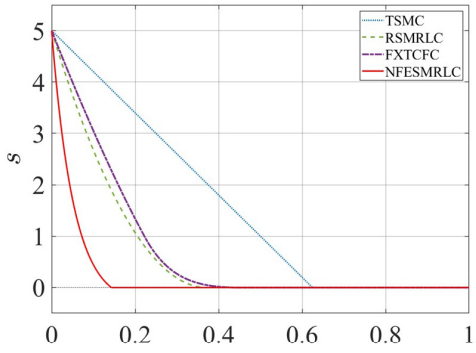


**FIGURE 2**. Performance comparison system state convergence process.

Derivation of Eq. (10) for the sliding mold surface yields:

$$\dot{s} = \dot{e} + ce + \mu\ddot{e} \tag{10}$$

Using the new reaching law of the design and combining Eq. (7) to Eq. (10), the expression for the current reference value $i_q^*$ of the speed controller can be derived as:

$$i_q^* = \frac{2J}{3p_n\psi_f}\left[\dot{\omega}_{ref} + \frac{B}{J}\omega_m + \frac{1}{J}d(t) + ce + \mu\ddot{e}dt + f(x)\tanh(\lambda s) + k|s|e^{(-\eta x)}\right] \tag{11}$$

Analyzing Eq. (11) shows that the total perturbation of the system is fed back to the control law as a known variable that affects the control performance. However, in the process of practical application, the total disturbance of the system $d(t)$ is not measurable. A comparison of the approaching speeds to the sliding mode surface is presented in Figure 2. The proposed NFESMRL exhibits superior performance, demonstrating the most rapid convergence among the TSMC, a reference sliding mode reaching law controller [1] (RSMRLC), and fixed-time command filter control [22] (FXTCFC).

### 3.2. Proof of Stability

To prove the stability of the NFESMRL-based speed controller system, the Lyapunov stability theorem is chosen to prove it by constructing a Lyapunov function of the following form.

$$V = \frac{1}{2}s^2 \tag{12}$$

Derivation of Eq. (12):

$$\dot{V} = s\dot{s} = -s\left[f(x)\tanh(\lambda s) + k|s|e^{(-\eta x)}\right] \tag{13}$$

The formulas $f(x)$ are all positive constants; the reaching terms $k$, $\eta$ are also positive constants; and the hyperbolic tangent function $\tanh(\lambda s)$ has positive and negative properties consistent with the sign function such that Eq. (6) satisfies the following conditions.

$$\dot{V} \leq 0 \tag{14}$$

When the initial operating condition of the system satisfies $s(0) > 1$, the finite-time calculation conducted on it shall be implemented in two stages.

Process 1: In $s(0) \to s = 1$ process, where $s \geq 1$, $\tanh(\lambda s) = 1$, when $t = 0$, $e^{-\eta t} = 1$. The sliding mode law can be approximated as $\dot{s} \approx -f(x) - ks$.

Assuming $\exists f_0 > 0$, $f(x) \geq f(0)$ holds for all $x$, the sliding mode law can be approximated as

$$\dot{s}_1 \leq -f_0 - ks \tag{15}$$

The convergence time of the state variables can be derived by integrating Eq. (15) as:

$$t_1 = \frac{1}{k}\ln\left(\frac{f_0 + k\cdot s(0)}{f_0 + k}\right) \tag{16}$$

Process 2: In $s = 1 \to s(0)$ process, where $\tanh(\lambda s) \approx \lambda s$, and $e^{-nt}$ decay exponentially, the sliding mode law can be approximated as

$$\dot{s}_2 = -f(x)\lambda s - ks = -s(f_0\lambda + k) \tag{17}$$

The convergence time of the state variables can be derived by integrating Eq. (17) as:

$$t_2 = \frac{1}{f_0\lambda + k + \eta}\ln\left(\frac{f_0\lambda + k + \eta}{f_0\lambda + k}\right) \tag{18}$$

The sum of the time required for the two processes is as:

$$t = \frac{1}{k}\ln\left(\frac{f_0 + k\cdot s(0)}{f_0 + k}\right) + \frac{1}{f_0\lambda + k + \eta}\ln\left(\frac{f_0\lambda + k + \eta}{f_0\lambda + k}\right) \tag{19}$$

where $t$ represents the cumulative convergence time of dominant power terms active during distinct operational stages. Finite-time convergence analysis ensures that the system state reaches equilibrium from any initial condition within a bounded time frame. Therefore, the actual NFESMRL convergence time is less than Eq. (19).

## 4. DESIGN OF THE DISTURBANCE OBSERVER

### 4.1. Disturbance Observer

Within the plant model given in Eq. (7), the total disturbance $d(t)$ is not directly measurable in practical applications. To enhance the controlled system performance and achieve online disturbance estimation, a sliding mode disturbance observer is pioneered. Based on the mechanical equations of motion of the permanent magnet synchronous motor, we select the mechanical angular velocity $\omega_m$ and total system perturbation $d(t)$ as state variables to derive the state-space equations:

$$\begin{cases} \dot{\hat{\omega}}_m = \frac{3p_n\psi_f}{2J} - \frac{B}{J}\hat{\omega}_m - \frac{1}{J}\hat{d}(t) + u_{smo} \\ \dot{\hat{d}}(t) = gu_{smo} \end{cases} \tag{20}$$

where $g$ is the feedback gain of the observer, $u_{smo}$ the switching signal, $\hat{\omega}_m$ the observed value of the mechanical angular velocity, and $\hat{d}(t)$ the observed value of the perturbation.

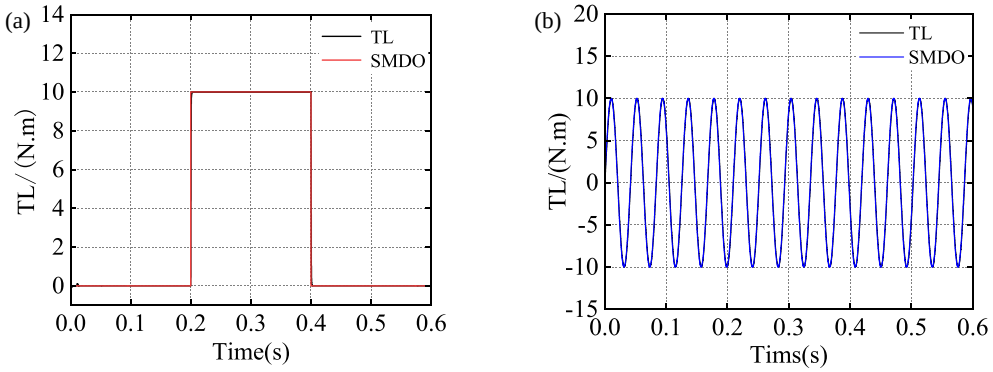


**FIGURE 3**. Observation diagram of load disturbance. (a) Rectangular waves. (b) Sine wave.

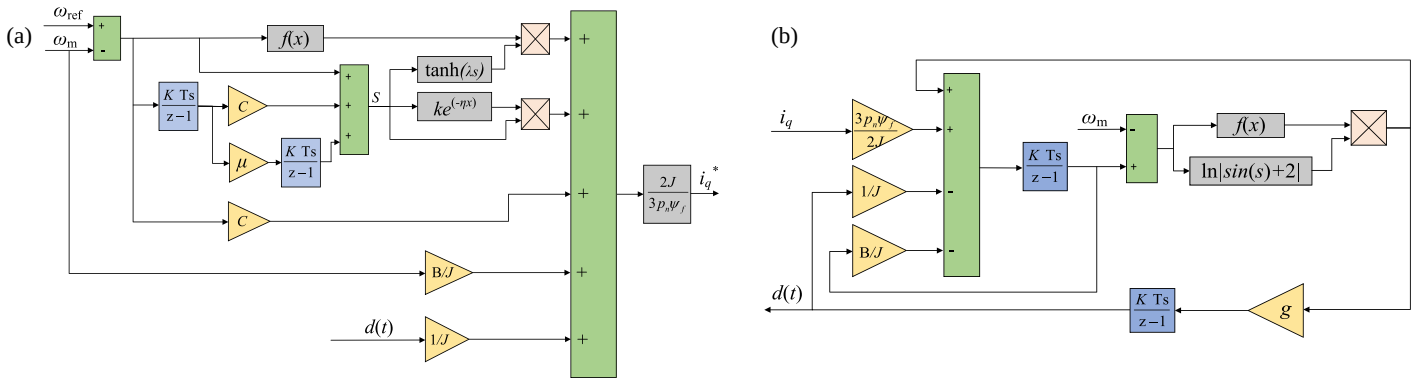


**FIGURE 4**. Schematic diagram of disturbance compensation. (a) Enhanced exponential reaching controller. (b) Disturbance compensation observer.

Based on Eq. (7) and Eq. (20), the sliding mode disturbance observer (SMDO) error equation is obtained:

$$\begin{cases} \dot{\tilde{\omega}}_m = -\frac{B}{J}\tilde{\omega}_m - \frac{1}{J}\tilde{d}(t) + u_{smo} \\ \dot{\tilde{d}}(t) = g u_{smo} \end{cases} \tag{21}$$

where $\tilde{\omega} = \hat{\omega} - \omega$ and $\tilde{d}(t) = \hat{d}(t) - d(t)$ are the estimation errors of velocity and total disturbance, respectively, and $u_{smo}$ is designed to be:

$$\begin{cases} u_{smo} = l f(s) \ln|\sin(s) + 2| \\ f(s) = \begin{cases} \frac{\varepsilon}{k}, & |s| \geq \delta \\ \frac{k|s|}{|s|^m + 1}, & |s| < \delta \end{cases} \end{cases} \tag{22}$$

A disturbance observer designed using Eq. (20) to (22) is used to estimate the total disturbance $d(t)$ of the system online, and the estimated total disturbance is compensated feedforward into the speed controller. The current reference $i_q^*$ of the speed controller can be expressed as:

$$i_q^* = \frac{2J}{3p_n\psi_f}\left[\dot{\omega}_{ref} + \frac{B}{J}\omega_m + \frac{1}{J}\hat{d}(t) + ce + \mu\ddot{e}dt + f(x)\tanh(\lambda s) + k|s|e^{(-\eta x)}\right] \tag{23}$$

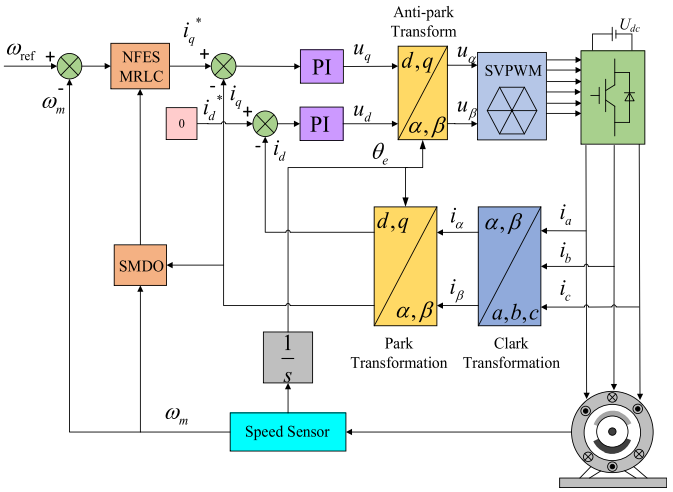


**FIGURE 5**. Block diagram of PMSM speed control system.

## 4.2. Performance Analysis

To provide a more intuitive assessment of the load disturbance observer's estimation accuracy, we conducted simulation comparisons under rectangular-wave and sinusoidal-wave load disturbances, with results shown in Figure 3. The rectangular-wave disturbance applied a 10 N·m load at 0.2 s and removed it at 0.4 s, while the sinusoidal disturbance had a 10 N·m amplitude and a period of 0.04 s. As seen in Figure 3(a), the disturbance estimates closely match their reference values, indicating the observer's effectiveness in tracking disturbance variations.

**TABLE 4.** Main PMSM parameters of the simulation.

| Symbol | Parameters | Value |
|---|---|---|
| $U_{dc}$ | DC voltage | 311 V |
| $\psi_f$ | Flux linkage | 0.175 Wb |
| $R_s$ | Stator resistance | 2.875 Ω |
| $J$ | Rotational inertia | 0.003 kg·m$^2$ |
| $B$ | Damping coefficient | 0.008 N·m·s |
| $L_s$ | $dq$-axis inductance | 8.5 mH |
| $P_n$ | Number of pole pairs | 2 |
| $n_N$ | Motor rated speed | 1500 rpm |
| $P_N$ | Rated Power | 1.5 KW |

**TABLE 5.** Main parameters of the simulation.

| Control strategy | Parameter value |
|---|---|
| TSMC | $k = 0.5, c = 0.01, \mu = 0.03$ |
| | $a = 2, \beta = 0.1$ |
| RSMRLC | $k = 0.5, m = 0.5, \alpha = 1.2$ |
| | $\eta = 25, c = 0.01, \lambda = 0.1$ |
| FXTCFC | $k = 0.5, m = 0.5, a = 2$ |
| | $\sigma = 0.5, \delta = 0.5, \beta = 0.1$ |
| NAESMRLC+SMDO | $k = 0.5, m = 0.5, \varepsilon = 1600$ |
| | $\eta = 25, c = 0.01, \lambda = 0.1$ |
| | $g = -1, \mu = 0.03, \delta = 0.1, l = 3.6$ |

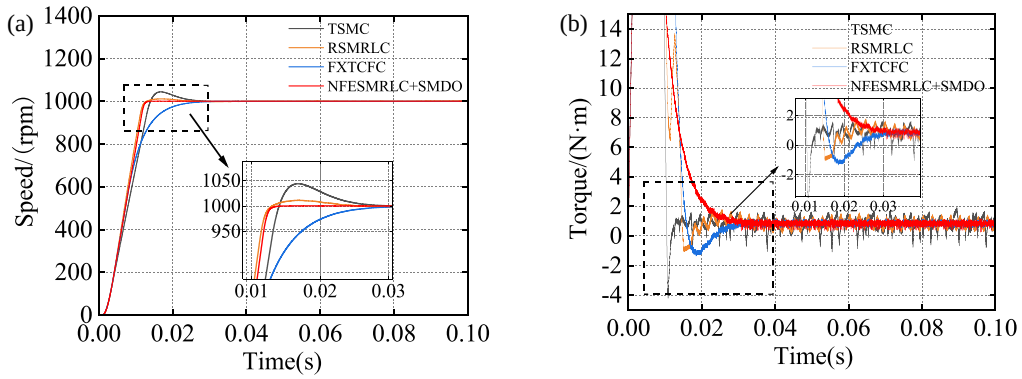


**FIGURE 6.** Startup simulation curve. (a) Speed waveforms. (b) Electromagnetic torque waveform.

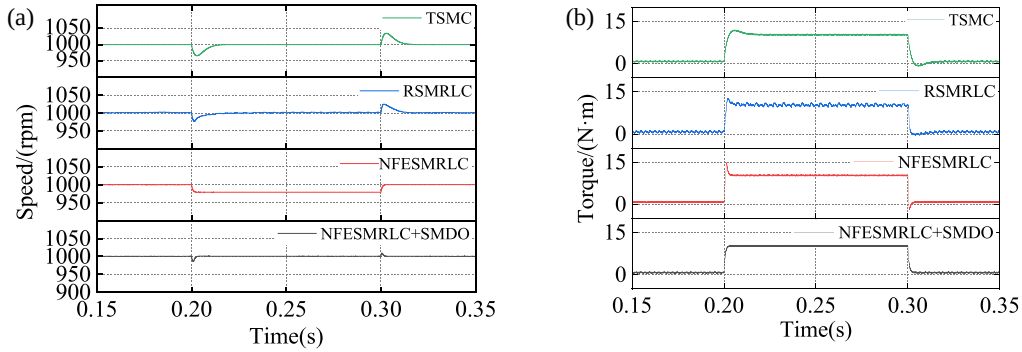


**FIGURE 7.** Load simulation curve. (a) Speed waveforms. (b) Electromagnetic torque waveform.

These estimated values are then fed back to the speed controller to compensate for speed drops.

## 5. SIMULATION AND EXPERIMENTAL ANALYSIS

The theory block diagram of PMSM speed regulation system with magnetic field orientation control is shown in Figure 4.

Simulations and experiments were conducted to compare the performances of four control schemes: a conventional sliding mode controller, RSMRLC, FXTCFC, and NFESMRL+SMDO.

### 5.1. Simulation Results and Analysis

#### 5.1.1. Startup Performance Analysis

To verify the dynamic response performance of the advanced enhanced exponential reaching law, simulations were conducted with a reference speed of 1000 rpm. The control system block diagram is shown in Figure 5. The speed and current waveforms for TSMC, RSMRLC, FXTCFC, and NFESMRLC+SMDO control strategies are shown in Figure 6. The PMSM parameters utilized in the simulation and control method parameters are enumerated in Table 4 and Table 5.

#### 5.1.2. Load Performance Analysis

To verify the anti-disturbance performance of the composite speed controller, simulations were conducted at 1000 rpm with a sudden 10 N·m load applied during 0.2–0.3 s. Speed and current waveforms under TSMC, RSMRLC, NFESMRLC, and NFESMRLC+SMDO strategies are shown in Figure 7.

Controllers with disturbance compensation show a minimal speed dip of 14 rpm. Controllers without compensation exhibit

**TABLE 6**. Comparison of simulation data.

| Control program | Startup process recovery | Speed overshoot | Sudden load recovery | Sudden load shedding recovery |
|---|---|---|---|---|
| TSMC | 0.08 s | 31.7% | 0.02 s | 0.018 s |
| RSMRLC | 0.025 s | 0.2% | 0.02 s | 0.014 s |
| NFESMRLC | 0.013 s | 0 | - | - |
| NFESMRLC+SMDO | 0.012 s | 0 | 0.003 s | 0.005 s |

31 rpm steady-state error. The $q$-axis current with compensation remains smoother and recovers rapidly after loading.

This confirms that the composite controller with disturbance compensation delivers superior anti-disturbance performance. Quantitative comparison data are provided in Table 6.

#### 5.1.3. Variable Speed Simulation Analysis

To verify the robustness of the control method, the reference speed was varied stepwise from 600 rpm to 800 rpm, then to 1000 rpm, and subsequently back to 800 rpm, before returning to 600 rpm. As shown in Figure 8, compared to the TSMC, RSMRLC, and FXTCFC methods, the NFESMRLC+SMDO exhibits no overshoot and faster recovery, demonstrating its superior robustness during variable-speed operation.

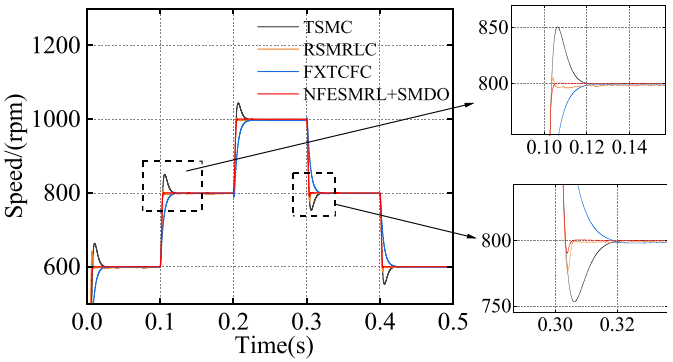


**FIGURE 8**. Simulation curve at variable speed.

### 5.2. Experimental Verification

The effectiveness of the proposed control method was validated on a dedicated experimental testbed for PMSM drive systems, as illustrated in Figure 9. The platform architecture comprises three primary subsystems: A 400 W surface-mounted PMSM with the following specifications: 3000 rpm rated speed, 0.25 Ω phase resistance, 0.5 mH $q$-axis inductance, 6.8 V·s/rad back-EMF constant, and one pole pair. A torque measurement unit incorporates a high-precision torque transducer. A load emulation subsystem uses a 48 V brushed DC motor with 12.5 A rated current.

The digital control implementation utilizes a TMS320F28335 digital signal processor (DSP) to execute real-time C-coded control algorithms with enhanced pulse width modulation (PWM) modulation techniques. The power stage configuration employs an IRS2103STRPBF three-phase gate driver featuring six-channel isolation, which

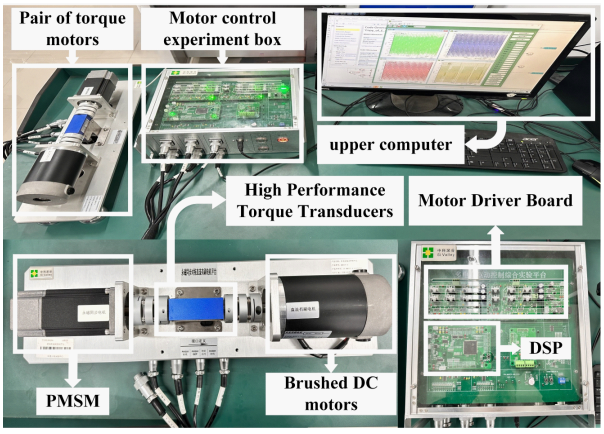


**FIGURE 9**. Experimental platform of permanent magnet synchronous motor drive control system.

drives twelve MOSFETs in a three-phase bridge topology for dual-motor actuation. Rotor position feedback is acquired via a 1024-line incremental optical encoder mounted on the PMSM shaft, achieving an angular velocity measurement resolution of 0.35°. Mechanical load profiles are dynamically generated through armature current regulation of the DC machine, enabling precise torque tracking within ±1.2% full-scale accuracy. Controller Sampling Time, Current loop: 50–100 μs, 10–20 kHz, Speed loop: 200–1000 μs, 1–5 kHz. The WTQ1050D dynamic miniature torque sensor, with a maximum rotational speed of 1800 rpm and a measurement range of 0–2 N·m, is interfaced with an AD7606 module that collects its output voltage signals at a maximum sampling rate of 200 Ksps.

Figure 10 compares experimental waveforms during no-load startup from 0 to 1000 rpm. The comparison of the effects of experimental results is as follows: NFESMRLC+SMDO achieves faster response with reduced steady-state torque pulsation than TSMC, FXTCFC, and RSMRLC. Measured response times: 0.12 s (NFESMRLC+SMDO), 3.1 s (FXTCFC), 0.65 s (RSMRLC), 1.2 s (TSMC). This demonstrates the presented method's effectiveness in improving system response speed.

Figure 11 compares the experimental waveforms under a step load increase operating condition at 1000 rpm. Figure 12 compares the experimental waveforms under a step load decrease operating condition at 1000 rpm. These results demonstrate NFESMRLC+SMDO's superior performance in minimizing speed deviations, reducing recovery time, and lowering torque transients, which confirms its enhanced anti-disturbance capability. Quantitative comparisons are provided in Table 7.

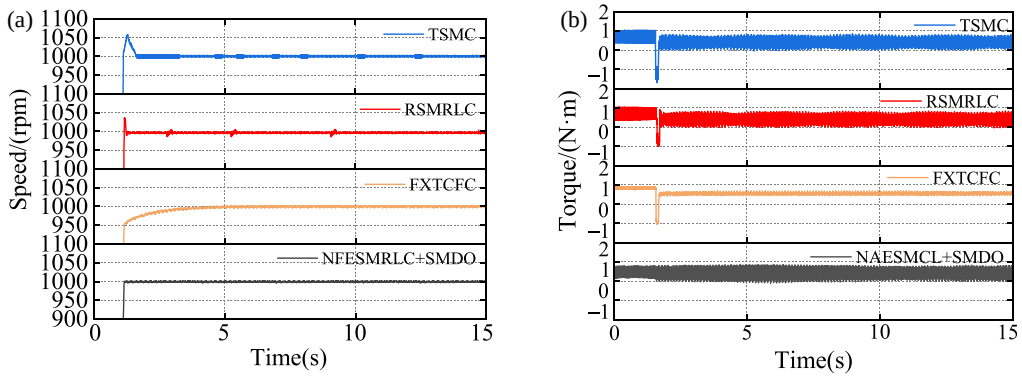


**FIGURE 10**. Comparison of experimental waveforms of speed and electromagnetic torque at no-load startup. (a) Speed waveforms. (b) Electromagnetic torque waveform.

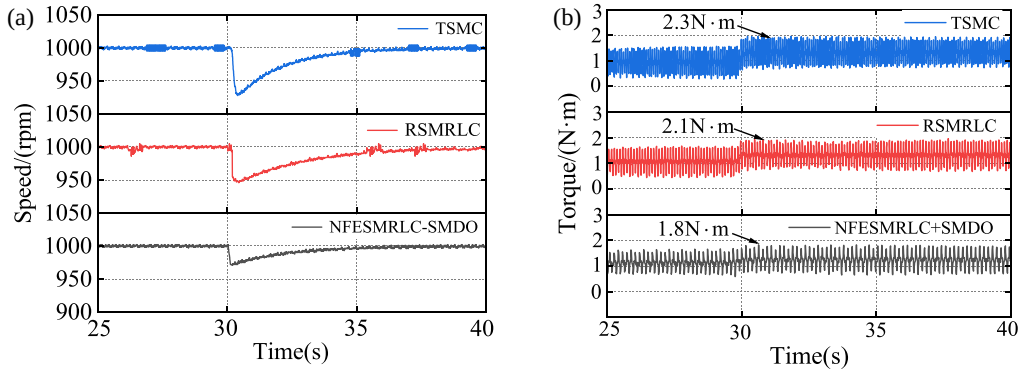


**FIGURE 11**. Comparison of experimental waveforms of rotational speed and electromagnetic torque during loading. (a) Speed waveforms. (b) Electromagnetic torque waveform.

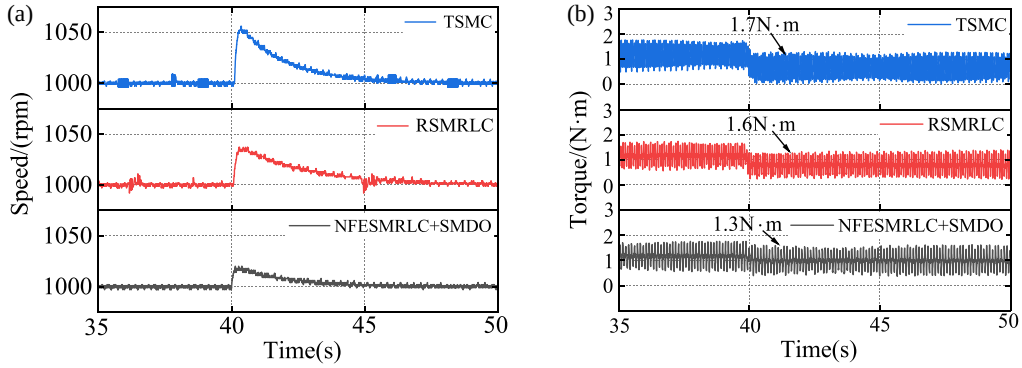


**FIGURE 12**. Comparison of experimental waveforms of rotational speed and electromagnetic torque at load reduction. (a) Speed waveforms. (b) Electromagnetic torque waveform.

**TABLE 7**. Comparison of experimental data.

| Control program | Speed arrival | Speed overshoot during startup | Sudden load recovery | Sudden load shedding recovery |
|---|---|---|---|---|
| TSMC | 1.2 s | 5.1% | 5 s | 4.8 s |
| RSMRLC | 0.65 s | 4.2% | 4.5 s | 3.9 s |
| NFESMRLC+SMDO | 0.12 s | 0% | 2.5 s | 2.1 s |

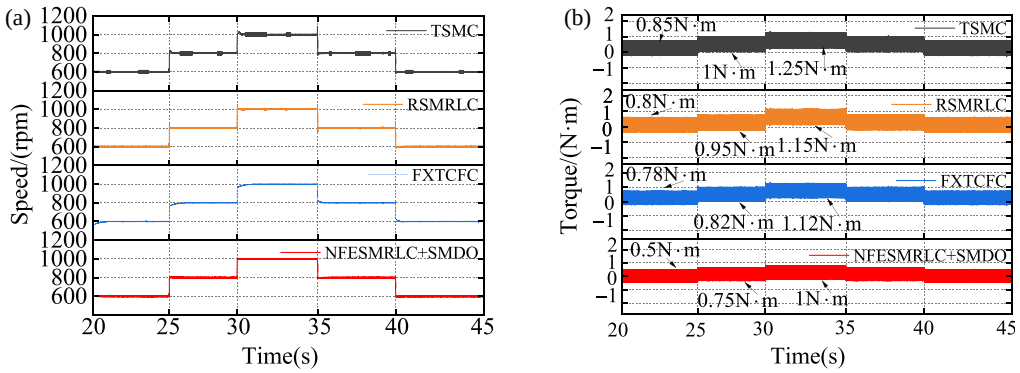


**FIGURE 13**. Comparison of experimental waveforms of rotational speed and electromagnetic torque at variable speeds. (a) Speed waveforms. (b) Electromagnetic torque waveform.

Figure 13 shows the comparison of the experimental waveforms of speed change from 600-800-1000-800-600 rpm. From Figure 13, it can be seen that NFESMRLC+SMDO has the fastest response, the smallest amount of overshooting, smoother waveforms, and the smallest fluctuation of the electromagnetic torque during the speed change. This verifies the rapidity and dynamics of the method. Moreover, the speed overshooting and torque errors of the method are smaller than those methods.

A further analysis of the NFESMRLC+SMDO control system under higher rotational speeds is presented in the next section. The speed tracking curve of the PMSM system controlled by NFESMRLC+SMDO is shown in Figure 14. The system maintains stable speed tracking within the 1000–1500 rpm range. Clearly, the controller demonstrates good adaptability in high-speed operating conditions.

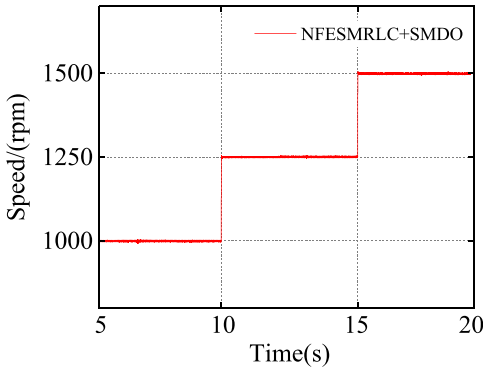


**FIGURE 14**. Control algorithm waveforms during variable-speed testing at rated speed.

## 6. CONCLUSION

This paper presents an integral sliding mode speed control strategy for PMSMs based on a fuzzy exponential reaching law. A newly developed fuzzy exponential reaching law for integral sliding mode control is introduced, which enhances the convergence rate while adaptively adjusting control gains through a fuzzy mechanism to effectively suppress chattering. Furthermore, a newly designed disturbance observer is implemented to enable real-time observation and compensation of load disturbances, significantly improving the system's robustness under complex operating conditions. Simulated and experimental results demonstrate marked advantages in both dynamic performance and disturbance rejection capability compared to conventional methods. The study has not yet completed performance verification at the motor's rated speed and higher operating ranges, and the control effectiveness and stability under high-speed conditions require further confirmation. Future work will primarily focus on conducting comprehensive experimental validation under rated and overload speed conditions to evaluate the control strategy's performance across the full speed range.

## ACKNOWLEDGEMENT

This work was supported in part by the Anhui Provincial Natural Science Foundation under Grant No. 2108085MF200, in part by the Natural Science Research Project of Anhui Educational Committee under Grant No. 2022AH051583, in part by the Anhui University of Technology Graduate Student Innovation Fund Project No. 2024cx2080.

## REFERENCES

[1] Zhang, Z., X. Yang, W. Wang, K. Chen, N. C. Cheung, and J. Pan, "Enhanced sliding mode control for PMSM speed drive systems using a novel adaptive sliding mode reaching law based on exponential function," *IEEE Transactions on Industrial Electronics*, Vol. 71, No. 10, 11 978–11 988, 2024.

[2] Saleh, S. A., E. Ozkop, B. Nahid-Mobarakeh, A. Rubaai, K. M. Muttaqi, and S. Pradhan, "Survivability-based protection for electric motor drive systems — Part II: Three phase permanent magnet synchronous motor drives," *IEEE Transactions on Industry Applications*, Vol. 59, No. 3, 2760–2771, 2023.

[3] Zhu, X., L. Zhang, X. Xiao, C. H. T. Lee, and H. Que, "Adjustable-flux permanent magnet synchronous motor sensorless drive system based on parameter-sensitive adaptive online decoupling control strategy," *IEEE Transactions on Transportation Electrification*, Vol. 9, No. 1, 501–511, 2023.

[4] Yu, Y., Y. Pei, F. Chai, and M. Doppelbauer, "Performance comparison between permanent magnet synchronous motor and vernier motor for in-wheel direct drive," *IEEE Transactions on Industrial Electronics*, Vol. 70, No. 8, 7761–7772, 2023.

[5] Wang, X., D. Wang, C. Peng, B. Wang, and X. Wang, "Torsional vibration analysis and suppression of interior permanent magnet synchronous motor with staggered segmented rotor for electric

vehicles," *IEEE Transactions on Transportation Electrification*, Vol. 10, No. 3, 6285–6294, 2024.

[6] Xu, J., W. Jin, H. Guo, and B. Zhang, "Improved optimal fault-tolerant control considering reluctance torque for five-phase IPMSM in aerospace electric actuation application," *IEEE Transactions on Industrial Electronics*, Vol. 71, No. 10, 11 785–11 795, 2024.

[7] Zhang, W., Y. Yang, M. Fan, L. He, A. Ji, Y. Xiao, H. Wen, X. Zhang, T. Yang, S. Mekhilef, and J. Rodriguez, "An improved model predictive torque control for PMSM drives based on discrete space vector modulation," *IEEE Transactions on Power Electronics*, Vol. 38, No. 6, 7535–7545, 2023.

[8] Chen, L., H. Zhang, H. Wang, K. Shao, G. Wang, and A. Yazdani, "Continuous adaptive fast terminal sliding mode-based speed regulation control of PMSM drive via improved super-twisting observer," *IEEE Transactions on Industrial Electronics*, Vol. 71, No. 5, 5105–5115, 2024.

[9] Zhang, S., A. Shen, X. Luo, Q. Tang, and Z. Li, "An adaptive strategy for PMSM-based disturbance estimation and online parameter identification," *IEEE/ASME Transactions on Mechatronics*, Vol. 29, No. 4, 2522–2533, 2024.

[10] Wang, F., L. He, J. Kang, R. Kennel, and J. Rodríguez, "Adaptive model predictive current control for PMLSM drive system," *IEEE Transactions on Industrial Electronics*, Vol. 70, No. 4, 3493–3502, 2023.

[11] Zhang, X., Z. Liu, P. Zhang, and Y. Zhang, "Model predictive current control for PMSM drives based on nonparametric prediction model," *IEEE Transactions on Transportation Electrification*, Vol. 10, No. 1, 711–719, 2024.

[12] Li, Z., Z.-H. Zhang, J.-S. Wang, Z.-B. Yan, X.-Q. Guo, and H.-X. Sun, "Nonsingular fast terminal sliding mode control strategy for PMLSM based on disturbance compensation," *Journal of Electrical Engineering & Technology*, Vol. 19, No. 3, 1331–1342, 2024.

[13] Huang, Z., M. Chen, and M. Lungu, "Interconnected disturbance observer-based tracking control for permanent magnet synchronous motors," *IEEE Transactions on Control Systems Technology*, Vol. 31, No. 6, 2953–2960, 2023.

[14] Wu, J., Y. Zhao, Y. Kong, Q. Liu, and L. Zhang, "Hierarchical nonsingular terminal sliding mode control with finite-time disturbance observer for PMSM speed regulation system," *IEEE Transactions on Transportation Electrification*, Vol. 10, No. 3, 4757–4765, 2024.

[15] Cheng, C., L. Liu, and S. Ding, "Iterative learning observer-based composite SOSM control for PMSM speed regulation problem with mismatched disturbances," *IEEE Transactions on Power Electronics*, Vol. 39, No. 8, 9470–9480, 2024.

[16] Liu, J.-F., Y. Feng, J.-Y. Yu, J.-W. Tang, and L. Zhang, "Fractional order second-order sliding mode MRASO for SPMSM," *Measurement and Control*, Vol. 57, No. 7, 863–870, 2024.

[17] Guo, X., S. Huang, Y. Peng, K. Lu, S. Huang, D. Luo, and X. Wu, "An improved integral sliding mode control for PMSM drives based on new variable rate reaching law with adaptive reduced-order PI observer," *IEEE Transactions on Transportation Electrification*, Vol. 9, No. 3, 4503–4516, 2023.

[18] Wang, L., J. Zhao, Z. Yu, Z. Pan, and Z. Zheng, "High-precision position control of PMLSM using fast recursive terminal sliding mode with disturbance rejection ability," *IEEE Transactions on Industrial Informatics*, Vol. 20, No. 2, 2577–2588, 2024.

[19] Qu, Y., B. Zhang, H. Chu, H. Shen, J. Zhang, and X. Yang, "Sliding-mode anti-disturbance speed control of permanent magnet synchronous motor based on an advanced reaching law," *ISA Transactions*, Vol. 139, 436–447, 2023.

[20] Kong, D., H. Cai, and H. Zhai, "Double-layer fast terminal sliding mode predictive control for PMSM speed regulation," *IEEE Journal of Emerging and Selected Topics in Power Electronics*, Vol. 12, No. 5, 4876–4887, 2024.

[21] Yim, J., S. You, Y. Lee, and W. Kim, "Chattering attenuation disturbance observer for sliding mode control: Application to permanent magnet synchronous motors," *IEEE Transactions on Industrial Electronics*, Vol. 70, No. 5, 5161–5170, 2023.

[22] Li, T., X. Chen, J. Liu, and J. Yu, "Fixed-time adaptive fuzzy control via filter and observer for uncertain nonlinear systems with disturbances and its application in PMSMs," *IEEE Transactions on Industrial Electronics*, Vol. 71, No. 11, 14 712–14 721, 2024.

[23] Liu, D., J. Han, G. Chen, Y. Cheng, X. Liang, and C. Song, "Fuzzy self-tuning fractional order PD permanent magnet synchronous motor speed control based on torque compensation," *Scientific Reports*, Vol. 15, No. 1, 2141, 2025.